Heat flux carried by the Antarctic Circumpolar Current mean flow

Che Sun

Geophysical Fluid Dynamics Laboratory/National Oceanic and Atmospheric Administration, Princeton, New Jersey, USA

D. Randolph Watts

Graduate School of Oceanography, University of Rhode Island, Narragansett, Rhode Island, USA

Received 18 October 2001; accepted 31 December 2001; published 6 September 2002.

[1] A stream function projection of historical hydrographic data is applied to study the heat flux problem in the Antarctic Circumpolar Current (ACC). The ACC is defined as a circumpolar band consisting of mean streamlines passing through Drake Passage. Its mean path exhibits a globally meandering pattern. The calculation of zonal heat transport shows that the ACC warms along its equatorward segments (South Atlantic and Indian Ocean) and cools along its poleward segment (South Pacific). The primary heat sources for the ACC system are two western boundary currents, the Brazil Current and the Agulhas Current. The mean baroclinic flow relative to 3000 dbar carries 0.14 PW poleward heat flux across 56°S and 0.08 PW across 60°S. *INDEX TERMS:* 1620 Global Change: Climate dynamics (3309); 4532 Oceanography: Physical: General circulation; 4536 Oceanography: Physical: Hydrography; *KEYWORDS:* ACC, heat flux, GEM

Citation: Sun, C., and D. R. Watts, Heat flux carried by the Antarctic Circumpolar Current mean flow, *J. Geophys. Res.*, *107*(C9), 3119, doi:10.1029/2001JC001187, 2002.

1. Introduction

[2] The Antarctic Circumpolar Current (ACC) connects the world oceans and plays a fundamental role in the global climate. The estimate of oceanic heat loss to the atmosphere south of 60°S is 0.5–0.6 PW (1 PW = 10^{15} Watts) [*Hastenrath*, 1982; *Gordon*, 1987], which must be balanced by oceanic poleward heat flux. There are two primary candidates: mean geostrophic flow (time-independent) and mesoscale eddies (transient). The widely held view that mesoscale eddies transport most of the heat in the Southern Ocean originated from *de Szoeke and Levine* [1981] (hereinafter referred to as DL81), who showed that mean geostrophic motions do not carry net heat flux across a circumpolar path of constant vertically averaged temperature.

[3] Direct heat flux calculations in the Southern Ocean have been based on the few synoptic hydrographic transects [e.g., *Georgi and Toole*, 1982; *Rintoul*, 1991]. In contrast, the circumpolar gravest empirical mode (GEM) method described by *Sun and Watts* [2001] (hereinafter referred to as SW2001) is able to utilize all synoptic and nonsynoptic historical casts by projecting data into a baroclinic stream function space. The three-dimensional GEM fields are parameterized by pressure, longitude, and geopotential height, and capture more than 97% of the total density and temperature variance in the ACC region. In a theoretical study that extends the Taylor-Proudman theorem to inhomogeneous fluids, *Sun* [2001a] shows that geostrophy leads to this remarkable GEM dominance.

0148-0227/02/2001JC001187$09.00

[4] To calculate advective heat flux from GEM fields, section 2 first introduces a mean streamline map to represent the ACC horizontal structure, from which a new definition of the ACC is adopted. The combination of GEM fields and the mean streamline map enables us to readily calculate the heat flux carried by the mean baroclinic flow.

2. Methods

2.1. Mean Streamline Map

[5] The ACC flow is approximately zonal in most parts of the Southern Ocean. At each longitude it displays temporal variability like meanders and meridional shifts. To describe the mean horizontal structure of the ACC, we produce a map of the baroclinic mass transport function relative to 3000 dbar

$$\Psi_{3000} = \int_0^{3000} \frac{p\delta}{g} dp, \tag{1}$$

where δ is specific volume anomaly and g is gravitational acceleration.

[6] The analysis uses a historical data set compiled by the Alfred Wegener Institute, covering the Southern Ocean between 30°S and 75°S (see SW2001 for a description of the data set, including the spatiotemporal distribution of stations). At each longitude the historical data within a longitudinal window of 10° width are used to generate a smoothing spline fit of Ψ_{3000} versus latitude. The 10° window is chosen in order to have adequate hydrographic casts for the smoothing procedure. Figure 1 shows examples at four longitudes.

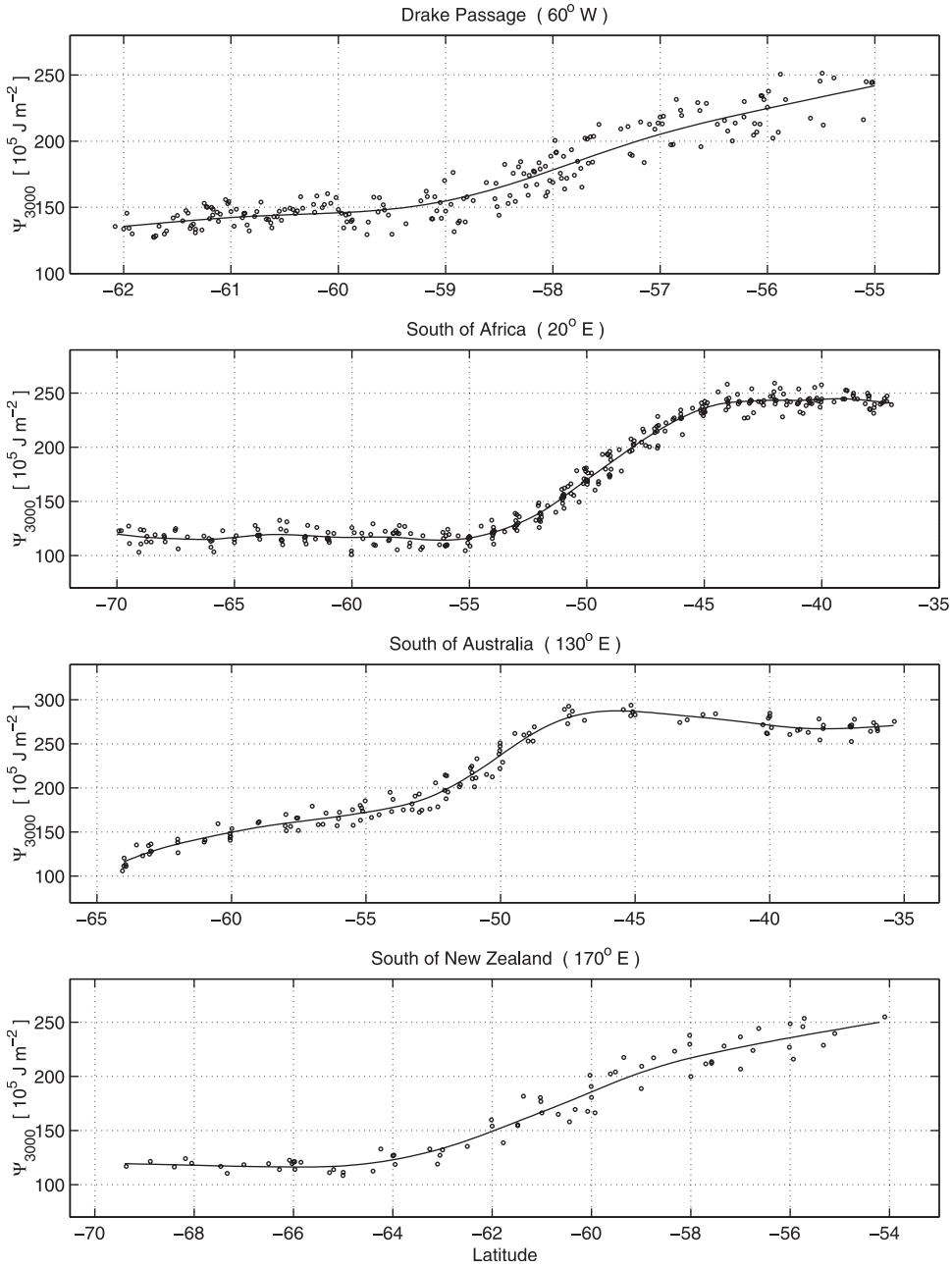

Figure 1. Spline-fit of Ψ_{3000} data taken from a longitudinal window of 10° width at each longitude.

[7] The circumpolar Ψ_{3000} field is plotted in Figure 2, which we call the mean streamline map (MSM). Many features in Figure 2 appear similar to the objective mapping product of *Olbers et al.* [1992]. However, the MSM scheme is much simpler because it implicitly utilizes the quasi-zonal character of the ACC and reduces the problem of smoothing the anisotropic circumpolar field to a series of one-dimensional procedure at each longitude.

2.2. Circumpolar Band

[8] Figure 2 reveals three different regimes in the Southern Ocean. The subpolar regime, with Ψ_{3000} values smaller than 130×10^5 J m^{-2}, consists of two cyclonic gyres in the Weddell Sea and the Ross Sea. The subtropical regime, with Ψ_{3000} values larger than 250×10^5 J m^{-2}, consists of subtropical gyres in three oceans with associated western boundary currents: the Brazil Current, the Agulhas Current and the East Australian Current. Part of the Agulhas water with Ψ_{3000} values of $250-280 \times 10^5$ J m^{-2} flows with the ACC into the South Pacific and may serve to balance the Indonesian Throughflow.

[9] Between the two regimes is a circumpolar band with Ψ_{3000} values of $140-240 \times 10^5$ J m^{-2}. The band is continuous around the globe and constricted by Drake Passage. Only within this band is the mean flow able to complete a circumpolar circle. We will define the ACC as this circumpolar band. A similar concept has appeared in *Orsi et al.* [1995], who noticed that the northern boundary of the ACC is approximately represented by the Subantarctic Front (SAF) and the southern boundary by the southern ACC Front.

[10] As will become clear later, the key to the success of our study lies in the definition of circumpolar band, which

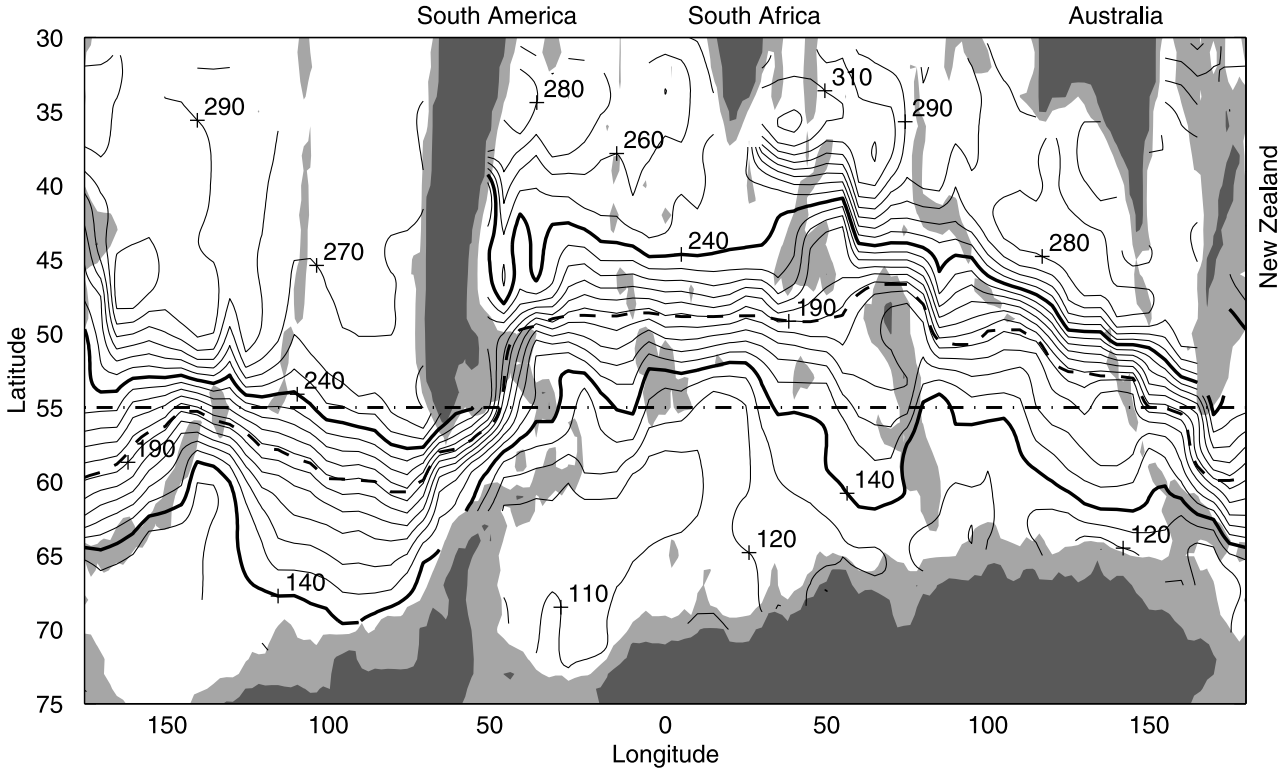

Figure 2. Mean streamline map for baroclinic mass transport function Ψ_{3000}. Contour interval is 10×10^5 J m^{-2}. The dash-dotted line is the ACC mean latitude at 55°S. The dashed curve represents the $\bar{\theta} = 2$°C path. The lightly shaded bathymetry is taken from ETOPO5 data and shallower than 3000 m.

effectively separates the ACC from the adjacent subtropical regime to the north and the subpolar regime to the south. The exact choice of the band is not crucial: it can be the transport function (as used here) or the geopotential height (as used by *Orsi et al.*), as long as they represent the mean streamlines passing through Drake Passage.

[11] The ACC mean path in Figure 2 exhibits a globally meandering pattern, deflecting equatorward east of Drake Passage and poleward south of New Zealand. The entire ACC is on the equator-side of its mean latitude (55°S) in the South Atlantic and in most of the south Indian Ocean, and on the polar-side in most of the South Pacific, a shift of more than 10° latitude. It is natural to expect that the ACC would warm along the equatorward segment and cool along the poleward segment due to interaction with neighboring waters and the atmosphere. If the mean temperature differs between the northward flow east of Drake Passage and the poleward flow south of New Zealand, the ACC mean flow would carry meridional heat flux across its mean latitude. The following study will test this hypothesis.

2.3. GEM Methodology

[12] The mean streamline map describes the geographic distribution of baroclinic stream function. The vertical thermohaline structure on each stream function contour is provided by the circumpolar GEM field. A combination of the two enables us to calculate the heat flux by the ACC baroclinic transport, as described below.

[13] Figure 3 shows a section at 140°E taken from the circumpolar GEM field. Because Ψ_{3000} can be calculated from the GEM δ field by SW2001 (which has been parameterized by geopotential height), it is a simple procedure to regrid the GEM fields onto a Ψ_{3000} coordinate by linear interpolation. The thermohaline features in the fields have been discussed by *Watts et al.* [2001]. For example the Polar Front (PF), characterized as the northern terminus of the subsurface temperature inversion, can be seen between 180 and 190 $\times$ 10^5 J m^{-2}.

[14] To calculate baroclinic heat transport, we divide the GEM field into a sufficiently small grid on the (Ψ, p) plane. The baroclinic mass transport function for a pressure interval (p_1, p_2) is derived in Appendix A as

$$\Psi - 12 = \int_{p_1}^{p_2} \frac{\Phi}{g} dp,$$

where geopotential Φ is relative to p_r = 3000 dbar. The baroclinic mass transport normal to each element is then determined by the horizontal difference of Ψ_{12},

$$M_{ij} = \triangle \Psi_{12} / f \tag{2}$$

in which (i, j) are grid number on the (Ψ, p) plane. The Coriolis parameter f is determined from the mean streamline map.

[15] The total heat transport across the section will be the sum over all elements:

$$Q_T = \sum_i^m \sum_j^n c_p \, \bar{\theta}_{ij} \, M_{ij} \tag{3}$$

where $\bar{\theta}_{ij}$ is the mean potential temperature on each element and c_p is the specific heat capacity of seawater. The heat calculation is relative to 0°C. If the total mass flux sums to

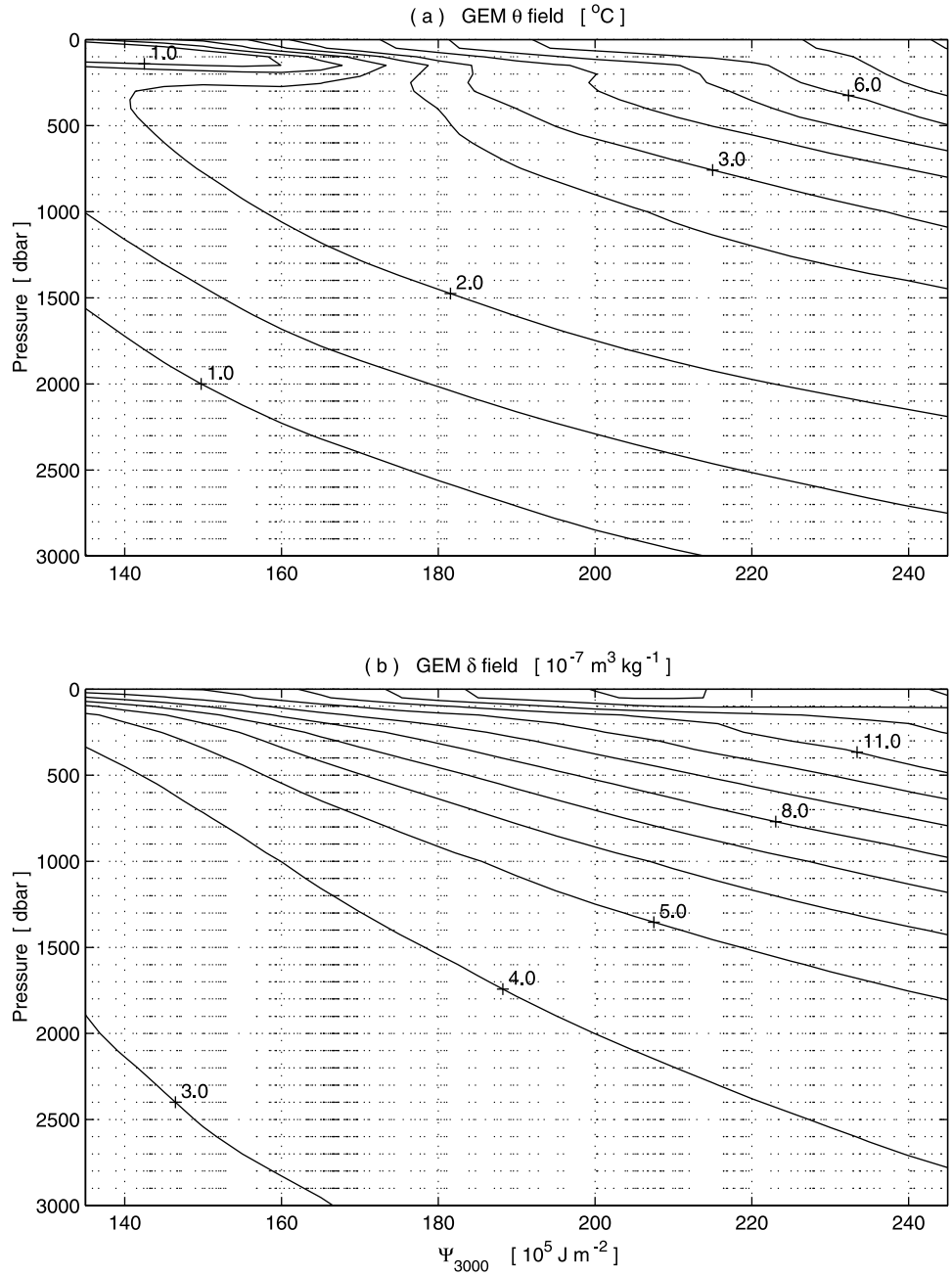

Figure 3. (a) GEM potential temperature field and (b) GEM specific volume anomaly field at 140°E (derived from SW2001). The superposed dotted lines represent historical casts used.

zero, the result is independent of reference temperature and can be called heat flux.

[16] Because the RMS residual σ_{ij} of the GEM potential temperature field is known, the error estimate for the heat flux calculation is

$$\sigma_T^2 = \sum_i^m \sum_j^n c_p^2 \, \sigma_{ij}^2 \, M_{ij}^2 \qquad (4)$$

[17] The method described above is suitable for studying the ACC because the large horizontal gradients associated with the ACC fronts are well resolved in stream function space. Traditional methods based on individual transects tend to introduce large error, because it is difficult to achieve adequate sampling in the frontal zone while trying to obtain a synoptic survey. For example, Figure 4 shows the Ψ_{3000} values from one hydrographic survey along 140°E. In the Polar Front Zone (Ψ_{3000} of 180–240 $\times$ 10^5 J m^{-2}) where large horizontal gradients exist, there were only two or three hydrographic casts. In comparison, the GEM field contains information from all available historical casts (more than 70 within the Polar Front Zone at this longitude) and therefore has higher resolution than individual transects.

3. Zonal Heat Transport

3.1. Heat Transport Calculation

[18] We apply the above method to GEM fields at each longitude, and calculate zonal heat transport within the

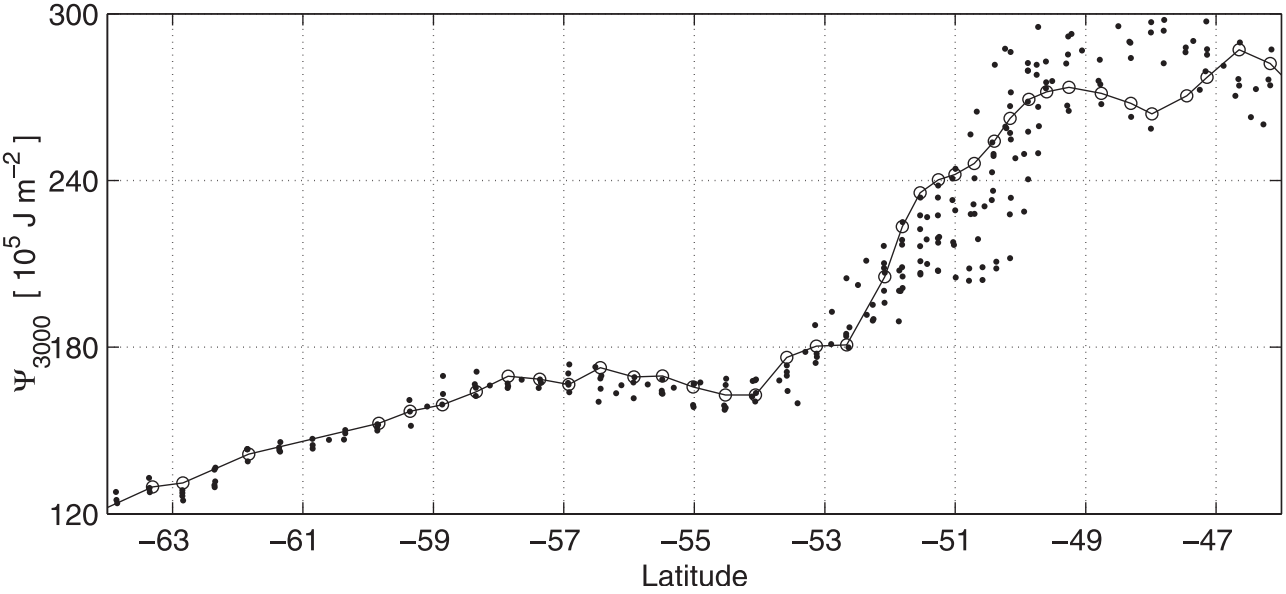

Figure 4. Ψ_{3000} values (circles) from one hydrographic survey along the WOCE SR3 line. Other historical casts used to generate the GEM field are shown as dots.

circumpolar band. The baroclinic transport between two Ψ_{3000} contours depends on their latitudes (via the Coriolis parameter). *Fofonoff* [1962] suggested that the mass transport is converted to, or from, the baroclinic mode when the flow shifts to different latitudes. To ensure constant mass transport within the circumpolar band, we add a barotropic component at each longitude. Here the barotropic component is defined as the velocity at the reference level (3000 dbar). Mooring observations in the ACC region suggest that the mean barotropic transport tends to follow the same direction of the baroclinic transport [*Nowlin et al.*, 1977].

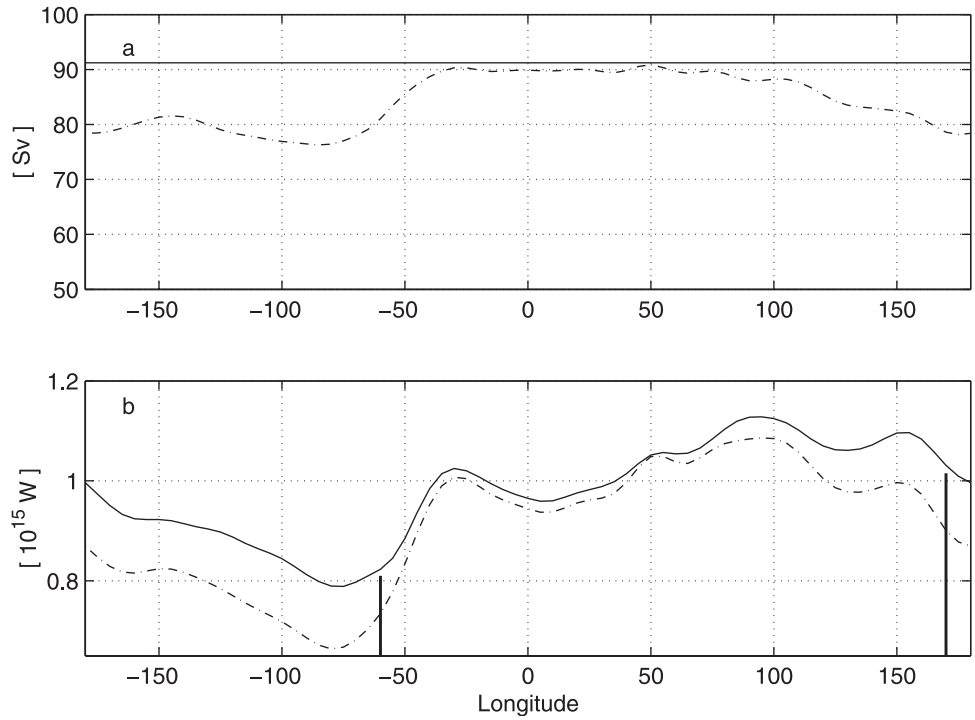

Figure 5. (a) Baroclinic transport within the circumpolar band (dashed line). The solid line represents a constant geostrophic transport. (b) Zonal heat transport within the ACC circumpolar band. The solid line corresponds to the constant geostrophic transport, and the dash-dotted line is the contribution from the baroclinic transport. Two bold vertical lines indicate the longitudes at Drake Passage and south of New Zealand.

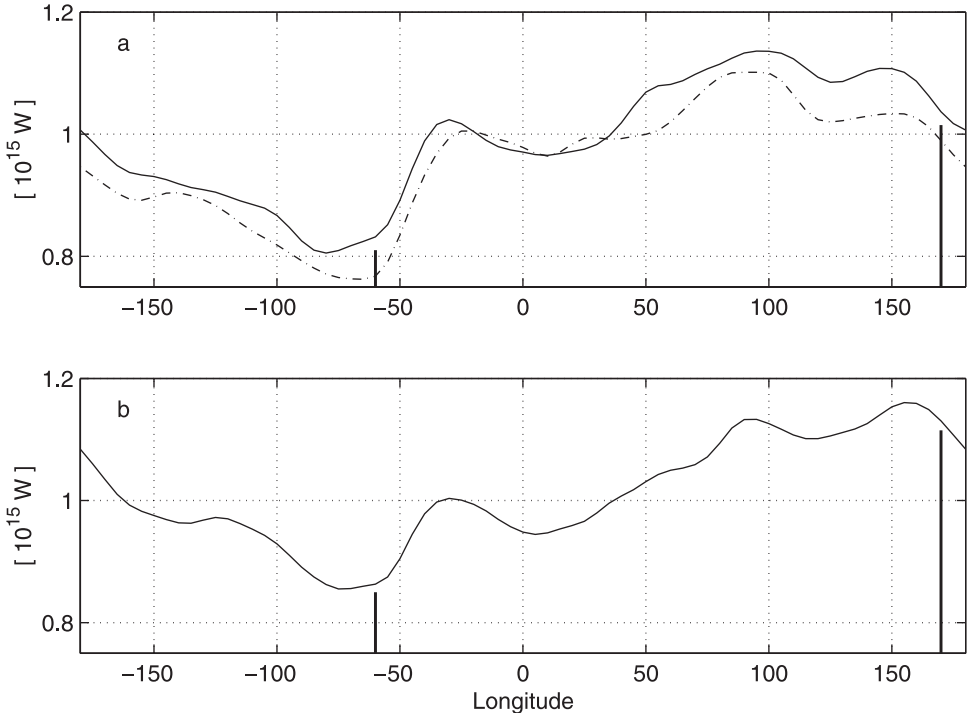

Figure 6. (a) Zonal heat transport in the warm season (solid line) and the cold season (dash-dotted line). (b) Zonal heat transport calculated by adjusting the northern boundary of the circumpolar band.

[19] The total transport within the circumpolar band is set to be the baroclinic transport at 50°E (91 Sv) where the ACC mean path is northernmost. The largest barotropic component is added at Drake Passage and constitutes about 15% of the total transport (Figure 5a). The ratio is close to what *Nowlin et al.* [1977] found in Drake Passage. Because of the thermal structure of the ocean, the barotropic component that advects vertically averaged temperature carries less heat flux than does the same amount of baroclinic transport (10–20% less).

[20] Figure 5b shows that the ACC zonal heat transport increases dramatically at the Brazil-Falkland Confluence (60°–40°W) and in the Agulhas Return Current region (30°–90°E), and decreases through the entire Pacific sector. The amplitude varies by about 0.35 PW. The averaged error (from equation (4)) is less than 0.007 PW due to the small RMS residual of the GEM fields. As we hypothesized, the ACC water warms up along the equatorward segments and cools along the poleward segment.

[21] The same calculation is then applied to the GEM fields generated from the warm season casts (November–April) and the cold season casts (May–October) separately. As shown in Figure 6a, the seasonal variation is only about 5% of the total zonal heat transport. Next we test whether the result is sensitive to the way that total mass flux is held constant. The calculation only includes the baroclinic component and the mass conservation is now achieved by slightly altering the northern limit of the band. Figure 6b shows that the heat transport value does change at each longitude, but the overall trend in each basin is the same.

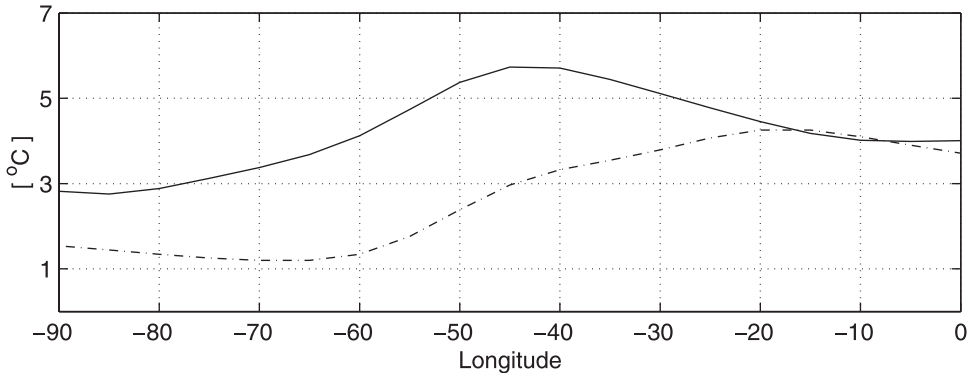

Figure 7. Mean surface temperature within the circumpolar band across the Brazil-Falkland Confluence. The solid line is calculated from the warm season GEM, and the dash-dotted line is from the cold season GEM.

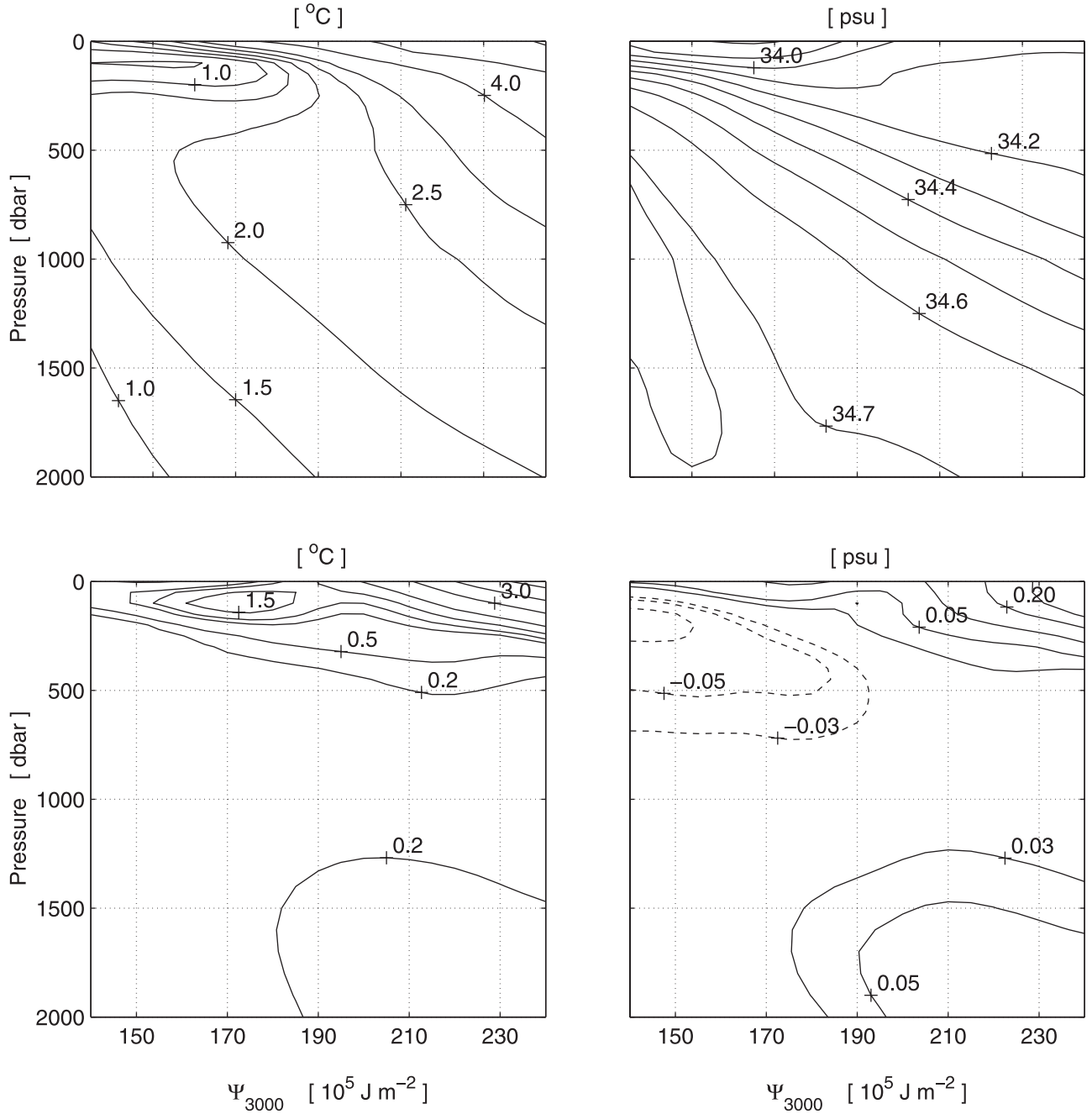

Figure 8. (top) Potential temperature and salinity fields at 60°W. (bottom) Difference of GEM field between section 60°W and section 40°W across the Brazil-Falkland Confluence (east minus west).

Irrespective of method, we find that the zonal heat transport at Drake Passage is about 0.2 PW less than that south of New Zealand.

3.2. Sources of Heat Input

[22] There are three sources that potentially contribute heat to the ACC system and cause the variation of zonal heat transport: atmosphere, surrounding subtropical waters, and western boundary currents. In Figure 5 the increase of ACC heat transport occurs in two confluence regions: the Brazil-Falkland Confluence and the Agulhas Return Current. Elsewhere the heat transport decreases slowly, suggesting that the input from surrounding subtropical waters is generally small.

[23] The dramatic cyclonic loop of the Falkland Current reaches as far north as 39°S, bringing the cold ACC water nearly 2000 km toward the warm subtropical region. One plausible assumption is that the increase of ACC heat transport comes from air-sea fluxes. This explanation may be rejected for three reasons. First, the map of air-sea heat flux by *Bunker* [1988] indicates a maximum of net annual heat gain by the ocean in the Falkland Current region. Simple calculation based on his value of 50 W m^{-2} shows that the net heat gain over the Falkland Current (50 W m^{-2} ×

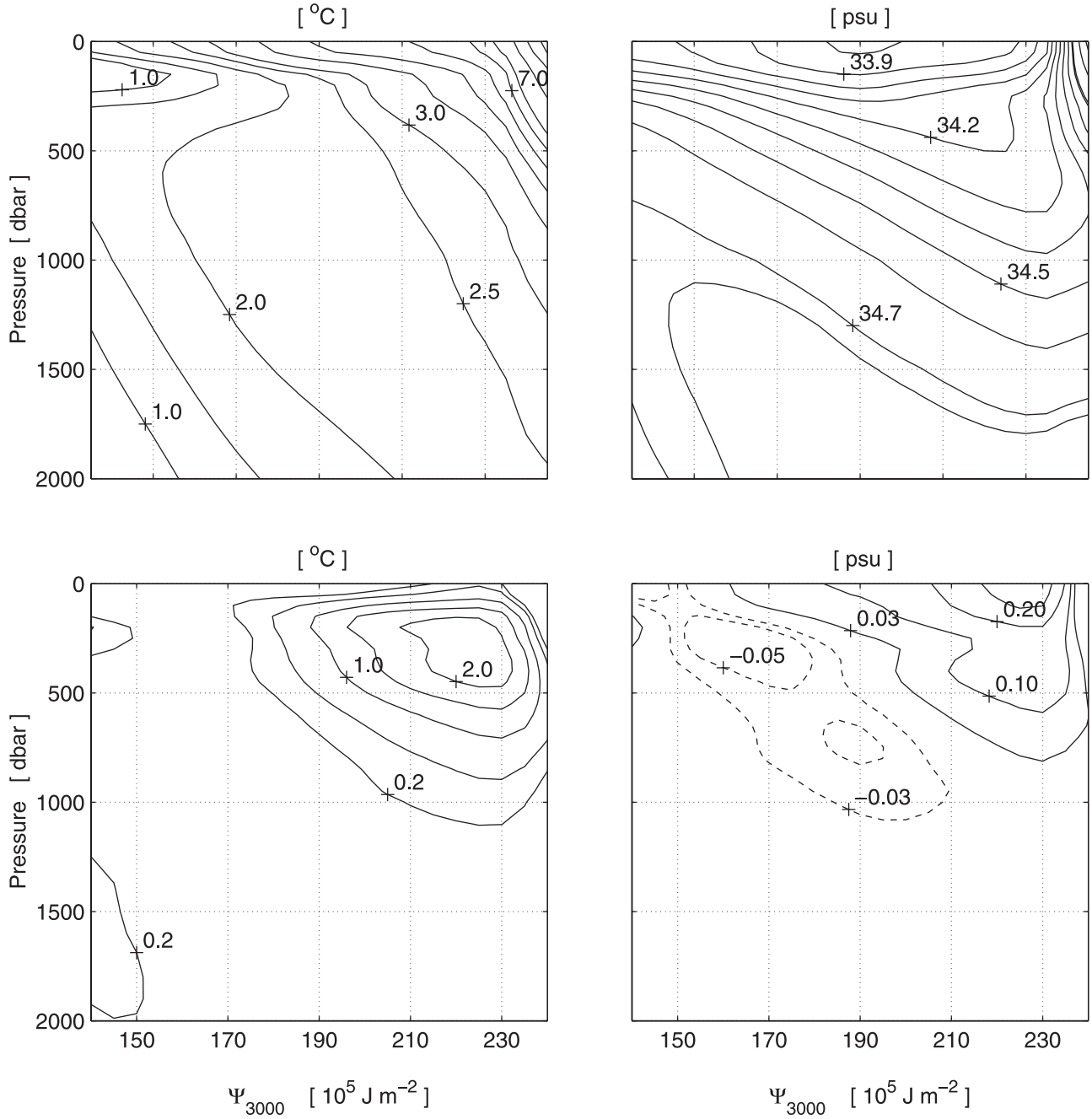

Figure 9. (top) Potential temperature and salinity fields at 30°E. (bottom) Difference of GEM field between section 30°E and section 90°E across the Agulhas Return Current (east minus west).

200 km × 2000 km = 0.02 PW) is one order of magnitude smaller than the increase of ACC zonal heat transport we see in Figure 5b. Second, in the cold season both heat transport (Figure 6a) and mean surface temperature (Figure 7) show a similar magnitude of increase across the confluence region as in the warm season, despite the net heat loss to the atmosphere during that season [see *Peterson and Stramma*, 1991, Figure 10]. Third, we examine in Figure 8 the difference between the water properties at the entering section (60°W) and the exiting section (40°W) of the confluence region. There are simultaneous temperature and salinity changes indicating the injection of warm and saline Brazil Current waters through the upper 500 dbar. All these support the idea that in the southwest Atlantic the ACC draws heat mainly from the Brazil Current.

[24] Similarly, the increase of ACC heat transport in the Indian Ocean sector (30°–90°E) comes from the warm Agulhas water. Figure 9 shows the difference of two GEM sections at 30° and 90°E which span the Agulhas Return Current region. The influence of the warm saline Agulhas water reaches as deep as 1000 dbar, dominating the northern half of the ACC (the Polar Front Zone between the SAF and the PF). The SAF and the Subtropical Front come very close in this sector and nearly merge in the Crozet Basin, which contributes to strong eddy activity and front-

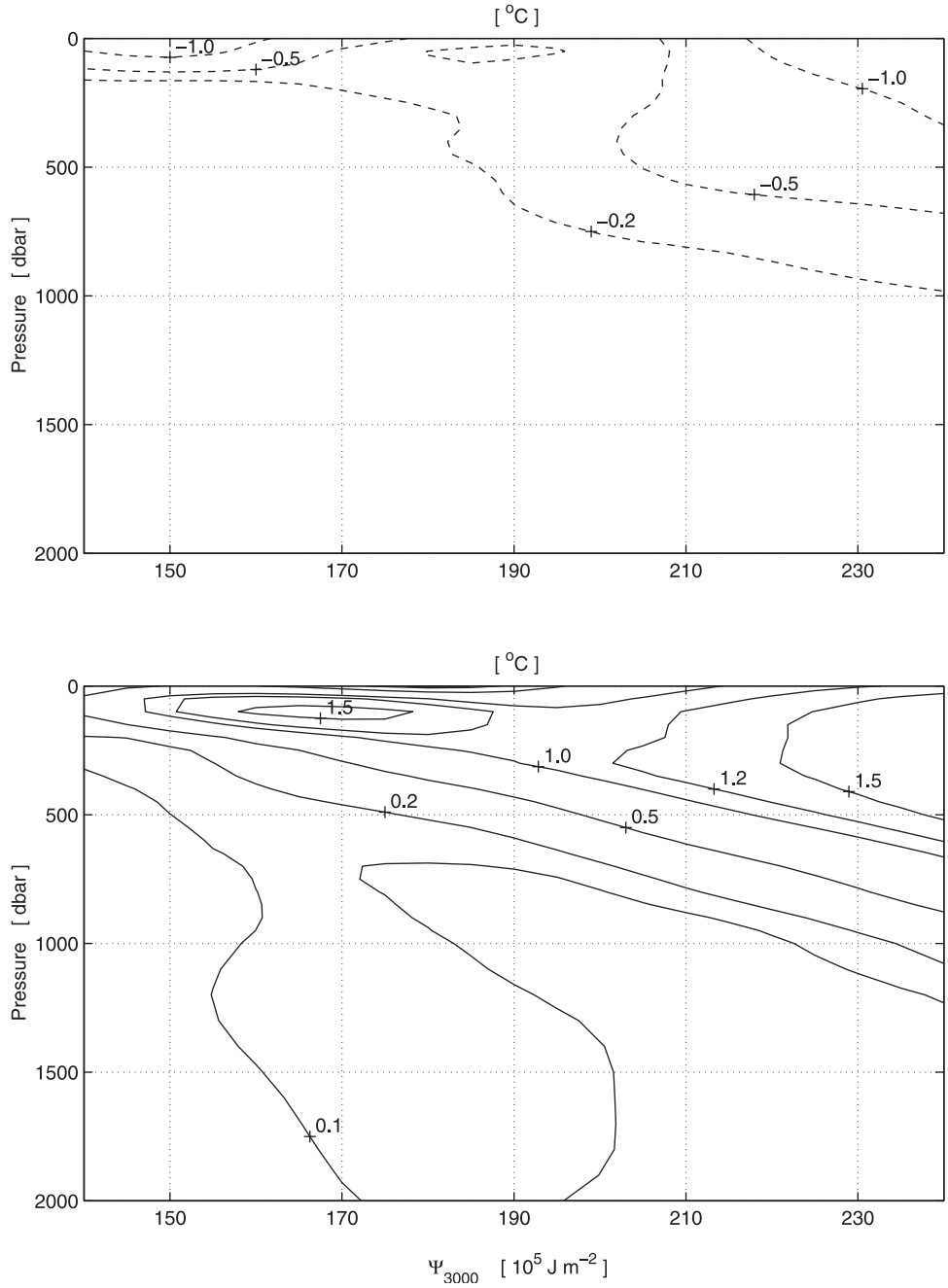

Figure 10. Difference of GEM potential temperature field (east minus west): (top) between section 150°W and section 90°W in the South Pacific and (bottom) between section 60°W at Drake Passage and section 170°E south of New Zealand.

front interaction. The latitude of the ACC band changes little across this region and the surface temperature remains fairly constant (Figure 9).

3.3. Comparison With Earlier Studies

[25] The finding that the ACC gains heat in the Atlantic and Indian Ocean sectors and loses heat in the Pacific sector differs from earlier studies. Both *Georgi and Toole* [1982] and *Rintoul* [1991] find that the ACC (defined differently) loses heat in crossing the Atlantic. Their studies use individual hydrographic transects and regard the ACC as the complete transect from South Africa to the Antarctic continent, in which case the ACC is not distinguished from neighboring subpolar and subtropical regimes.

[26] As the ACC traverses the South Pacific at relatively high latitudes, it gradually releases the heat gained from the Brazil Current and the Agulhas Current, either to the atmosphere or to neighboring polar waters. Despite strong eddy activity around the Mid-Pacific Ridge, Figure 10 (top) shows the cooling process with no indication of heat input from surrounding subtropical waters, which agrees with *Gille*'s [1999] inverse model study.

[27] The heat transport result in this study is robust because it reflects a change of the ACC internal mode,

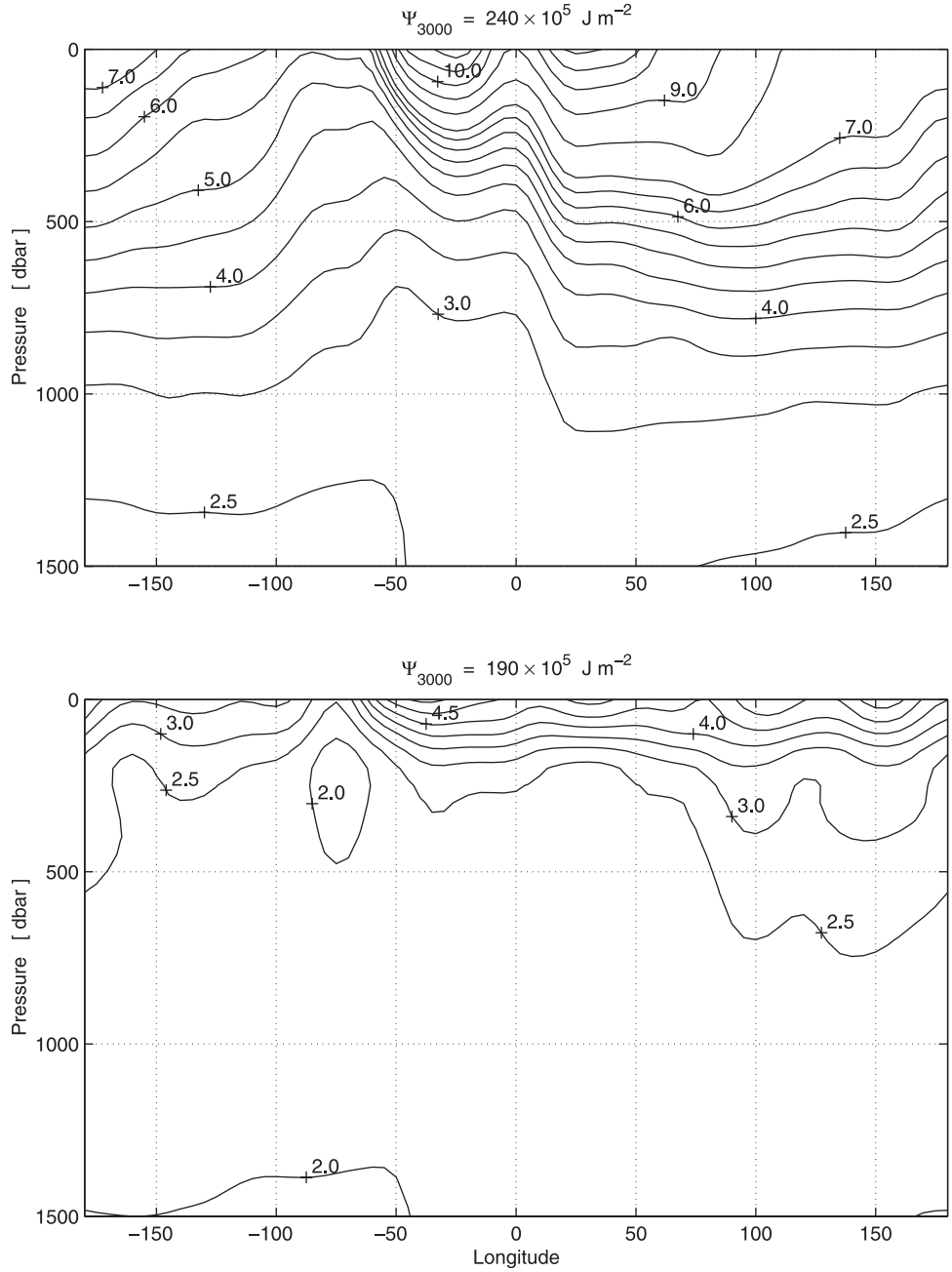

Figure 11. GEM potential temperature field along a stream function contour close to (top) the SAF and (bottom) the PF.

which is insensitive to the uncertain velocity field. The along-stream evolution of the ACC thermal structure, as depicted in Figure 11, is deep-reaching and well correlated to the heat transport variation. The thermal changes are particularly concentrated in the northern part of the ACC (near the SAF).

4. Poleward Heat Flux

4.1. Different Circumpolar Paths

[28] The ACC zonal heat transport south of New Zealand is 0.2 PW higher than that at Drake Passage (Figure 5b). In fact the whole water column south of New Zealand is warmer than that at Drake Passage (Figure 10, bottom), a phenomenon that becomes evident in a stream function view.

[29] Section 2.2 mentions that a zonal heat transport divergence should result in a net poleward heat flux across the mean latitude of the ACC. To demonstrate it, we directly calculate the net heat flux by the mean baroclinic flow normal to various circumpolar paths. The calculation is conducted in geographic space by combining the mean streamline map and the circumpolar GEM fields. The results are listed in Table 1.

(1) Streamline path. In the first case the path is along a mean streamline with constant Ψ_{3000}. The total baroclinic

Table 1. Poleward Heat Flux by the Baroclinic Flow Relative to 3000 dbar

Circumpolar Paths	Poleward Heat Flux, PW	Uncertainty, PW
$\Psi_{3000} = 240 \times 10^5$ Jm^{-2}	0.040	0.003
$\Psi_{3000} = 190 \times 10^5$ Jm^{-2}	−0.001	0.001
$\Psi_{3000} = 140 \times 10^5$ Jm^{-2}	−0.001	0.001
56°S latitude circle	0.140	0.010
58°S latitude circle	0.095	0.009
60°S latitude circle	0.082	0.008
$\bar{\theta} = 2$°C	−0.001	0.002

transport across this path is zero. Although individual elements at different depths along the section can have nonzero mass flux, the magnitude of cross-stream baroclinic transport summed for either direction is quite small (10 Sv). Three examples are calculated for Ψ_{3000} = 240, 190, and 140×10^5 J m^{-2}, roughly corresponding to the SAF, the PF, and the Southern ACC Front. Except for the northernmost streamline near the SAF, the meridional heat flux across the streamlines of the southern half of the ACC is trivial (less than 0.001 PW and below the error bar).

(2) Latitude path. In this case we choose latitudinal circles at 56°, 58°, and 60°S, all south of Cape Horn. A poleward heat flux of 0.14 PW is obtained at 56°S, consistent with the difference of zonal heat transport between the New Zealand section and the Drake Passage section. Note that the calculation of zonal heat transport is conducted in stream function space and has higher resolution. For latitudinal circles further south, the poleward heat flux decreases and reaches 0.08 PW at 60°S.

(3) Temperature path. To compare with DL81, we choose a circumpolar path that has constant vertically averaged potential temperature ($\bar{\theta}$ = 2°C, average between 0–3000 dbar) and meanwhile closely follows the PF. The barotropic motions carry zero heat flux across this path. The poleward heat flux by mean baroclinic motions is -0.001 ± 0.002 PW. DL81 obtain a similar result but with larger error bounds (0 ± 0.23 PW). They conclude that mean geostrophic motions do not carry heat across the ACC and eddy heat flux is the prime candidate for compensating heat loss south of the ACC.

4.2. Heat Flux Across the ACC

[30] Figure 2 shows that the temperature path, being chosen to follow the PF, is close to the stream function contour of $\Psi_{3000} = 190 \times 10^5$ J m^{-2}. This agrees with the front-tracking study by *Sun* [2001b], which finds that the PF position nearly follows a stream function contour. It is not surprising that there is little heat flux by mean flows across such a quasi-streamline path.

[31] The study by DL81 has been widely cited to support the view that mesoscale eddies, instead of the ACC mean flow, carry poleward heat flux in the Southern Ocean. Our study shows that the view needs to be clarified: while it is correct to say that mean geostrophic motions carry little heat flux across the ACC (i.e., across a streamline path), the result can not be generalized to other circumpolar paths, such as a latitudinal circle. The case 2 and case 3 in section 4.1 would only be equivalent if the ACC were a pure zonal flow. It is not appropriate to assess the role of ACC mean flow solely based on quasi-streamline paths, because the important effect of the ACC globally meandering path is missing from the picture. A similar view has been expressed by *Thompson* [1993] in his analysis of the FRAM model output.

[32] Indeed, our calculation shows that at 56°S the mean baroclinic flow relative to 3000 dbar contributes about 0.14 PW poleward heat flux. If the observation at Drake Passage [*Nowlin et al.*, 1977] is typical of the ACC, baroclinic transport relative to 3000 dbar should constitute about 80% of the total transport, in which case the estimate of 0.14 PW can be increased by as much as 20% to account for the combined baroclinic and barotropic mean flow.

4.3. Other Components

[33] The present study addresses only one part of the oceanic heat flux. Other components, including Ekman flux and eddy heat flux, can be studied indirectly because their accumulative effect is reflected in the downstream evolution of the GEM field and partly contributes to the variation of zonal heat transport. The topic will be explored in a future study.

[34] The meridional shift of the mean path and the intensive interaction with two western boundary currents suggest that the ACC, especially its northern half, is not a closed system and has a significant zonally asymmetric component. Unlike its atmospheric counterpart, the ACC may not even have a proper zonally symmetric component based on the Eulerian mean in Figure 2. Therefore using channel model and zonal mean theory to describe the ACC is questionable.

5. Summary

[35] A stream function projection method, the circumpolar gravest empirical mode, enables us to study the heat flux problem in the Southern Ocean using all available historical data. A circumpolar band constricted by Drake Passage is used to define the ACC, which separates it from surrounding subtropical and subpolar regimes. The ACC under this definition exhibits a circumpolar standing meander pattern.

[36] The zonal heat transport within the circumpolar band increases in the South Atlantic and Indian Ocean sectors (equatorward segments), and decreases across the South Pacific sector (poleward segment). The entire water column south of New Zealand is warmer than that at Drake Passage. Through its globally meandering path, the ACC mean flow continuously transports heat from warm subtropical regions to cold subpolar regions. The primary heat sources for the ACC system are found to be the Brazil Current and the Agulhas Current, instead of the atmosphere or surrounding warm subtropical waters.

[37] The study confirms that mean geostrophic motions transport little heat flux across a mean streamline path or a path with constant vertically averaged temperature, in agreement with DL81. The mean baroclinic flow relative to 3000 dbar, however, carries 0.14 PW poleward heat flux across the 56°S latitudinal circle and 0.08 PW across 60°S. It is the first time a study based on hydrographic data demonstrates that the ACC mean flow carries poleward heat flux in the Southern Ocean.

[38] The stream function projection we introduced is also applicable to the general circulation of the atmosphere, and should be compared with various Lagrangian mean diagnostics [e.g., *Nakamura*, 1995]. In another study we further apply the method to diagnose the low-frequency variability in strong baroclinic currents [*Sun and Watts*, 2002].

Appendix A: Baroclinic Mass Transport Function

[39] In order to calculate mass flux across a small element on the vertical section, we derive a form of mass transport function for arbitrary pressure intervals. The geostrophic relation in isobaric coordinates is

$$f\ u_g = -\frac{\partial \Phi}{\partial y},\ f\ v_g = \frac{\partial \Phi}{\partial x} \tag{A1}$$

The baroclinic part of geopotential is defined as

$$\Phi = -\int_{p_r}^{p} \delta\ dp \tag{A2}$$

in which

$$\delta = \frac{1}{\rho(S,T,p)} - \frac{1}{\rho(35,0,p)} = \alpha - \alpha_0$$

and α is specific volume.

[40] After applying the hydrostatic approximation $dp = -\rho g\ dz$, the mass transport per unit width integrated over a pressure interval (p_1, p_2) becomes

$$\int_{z_2}^{z_1} \rho u_g\ dz = -\int_{p_2}^{p_1} \frac{u_g}{g}\ dp = \frac{1}{f}\frac{1}{\partial y}\int_{p_2}^{p_1} \frac{\Phi}{g} dp = -\frac{1}{f}\frac{\partial \Psi_{12}}{\partial y}, \tag{A3}$$

and

$$\int_{z_2}^{z_1} \rho v_g\ dz = -\int_{p_2}^{p_1} \frac{v_g}{g}\ dp = \frac{1}{f}\frac{1}{\partial x}\int_{p_2}^{p_1} \frac{\Phi}{g} dp = -\frac{1}{f}\frac{\partial \Psi_{12}}{\partial x} \tag{A4}$$

which gives a baroclinic mass transport function as

$$\Psi_{12} = \int_{p_1}^{p_2} \frac{\Phi}{g} dp. \tag{A5}$$

[41] For a small interval on which the Coriolis parameter is nearly constant, the horizontal integration of mass transport function gives rise to the baroclinic mass flux across the element as $\Delta\ \Psi_{12}/f$, where Δ represents the horizontal difference of Ψ_{12} between the two ends of the interval.

Appendix B: Potential Energy Anomaly

[42] The baroclinic mass transport function we introduced is different from potential energy anomaly (the so-called Fofonoff potential). The potential energy for a pressure interval is

$$E_p = \int_{z_2}^{z_1} p\ dz = \int_{p_1}^{p_2} \frac{p\alpha}{g} dp = \int_{p_1}^{p_2} \frac{p\alpha_0}{g} dp + \int_{p_1}^{p_2} \frac{p\delta}{g} dp = E_p^0 + \chi_{12},$$

where E_p^0 is a function of p_1 and p_2 only. Potential energy anomaly is

$$\chi_{12} = \int_{p_1}^{p_2} \frac{p\delta}{g} dp. \tag{B1}$$

To find the relation between χ_{12} and mass transport function, we expand (A5),

$$\Psi_{12} = \int_{p_1}^{p_2} \frac{\Phi}{g} dp = \frac{p\Phi}{g}\Big|_{p_1}^{p_2} - \int_{p_1}^{p_2} \frac{p}{g} d\Phi = \frac{p_2\Phi(p_2)}{g} - \frac{p_1\Phi(p_1)}{g} + \chi_{12} \tag{B2}$$

For the water column between surface and the reference level, the first two terms vanish and mass transport function is identical to the potential energy anomaly defined by *Fofonoff* [1962], i.e.,

$$\Psi = \chi = \int_0^{p_r} \frac{p\delta}{g} dp. \tag{B3}$$

For an arbitrary pressure interval, however, potential energy anomaly χ_{12} is not a stream function and cannot be used to calculate mass transport.

[43] **Acknowledgments.** The historical hydrographic data used in this study were kindly provided by the Alfred Wegener Institute. Helpful comments from Tom Rossby, Peter Cornillon, John Merrill, Kirk Bryan and three anonymous reviewers are appreciated. The SAFDE program is supported by the National Science Foundation under Grants OCE-95-04041 and OCE-99-12320.

References

Bunker, A. F., Surface energy fluxes of the South Atlantic Ocean, *Mon. Weather Rev.*, *116*, 809–823, 1988.

de Szoeke, R. A., and M. D. Levine, The advective flux of heat by mean geostrophic motions in the Southern Ocean, *Deep Sea Res., Part I*, *28*, 1057–1085, 1981.

Fofonoff, N. P., Dynamics of ocean currents, in *The Sea*, vol. 1, edited by M. Hill, pp. 323–396, Interscience, New York, 1962.

Georgi, D. T., and J. M. Toole, The Antarctic Circumpolar Current and the oceanic heat and freshwater budgets, *J. Mar. Res.*, *40*, (suppl.), 183–197, 1982.

Gille, S. T., Mass, heat, and salt transport in the southeastern Pacific: a circumpolar current inverse model, *J. Geophys. Res.*, *104*, 5191–5209, 1999.

Gordon, A. L., Polar Oceans, *Rev. Geophys*, *25*, 227–233, 1987.

Hastenrath, S., On meridional heat transport in the world ocean, *J. Phys. Oceanogr.*, *12*, 922–927, 1982.

Nakamura, N., Modified Lagrangian-mean diagnostics of the stratospheric polar vortices, part I, Formulation and analysis of GFDL SKYHI GCM, *J. Atmos. Sci.*, *52*, 2096–2108, 1995.

Nowlin, W. D., Jr., T. Whitworth III, and R. D. Pillsbury, Structure and transport of the Antarctic Circumpolar Current at Drake Passage from short-term measurements, *J. Phys. Oceanogr.*, *7*, 788–802, 1977.

Olbers, D., V. Gouretski, G. Seiß, and J. Schröter, *Hydrographic Atlas of the Southern Ocean*, Alfred Wegener Inst., Bremerhaven, Germany, 1992.

Orsi, A. H., T. Whitworth III, and W. D. Nowlin Jr., On the meridional

extent and fronts of the Antarctic Circumpolar Current, *Deep Sea Res., Part I*, *42*, 641–673, 1995.

Peterson, R. G., and L. Stramma, Upper-level circulation in the South Atlantic Ocean, *Prog. Oceanogr.*, *26*, 1–73, 1991.

Rintoul, S. R., South Atlantic interbasin exchange, *J. Geophys. Res.*, *96*, 2675–2692, 1991.

Sun, C., The columnar structure in stratified geostrophic flows, *Geophys. Astrophys. Fluid Dyn.*, *95*, 55–65, 2001a.

Sun, C., A study of the Antarctic Circumpolar Current in streamfunction space, Ph.D diss., 178 pp., Grad. School of Oceanogr., Univ. of R. I., Narragansett, 2001b.

Sun, C., and D. R. Watts, A circumpolar gravest empirical mode for the Southern Ocean hydrography, *J. Geophys. Res.*, *106*, 2833–2856, 2001.

Sun, C., and D. R. Watts, A pulsation mode in the Antarctic Circumpolar Current south of Australia, *J. Phys. Oceanogr.*, *32*, 1479–1495, 2002.

Thompson, S. R., Estimation of the transport of heat in the Southern Ocean using the Fine-Resolution Antarctic Model, *J. Phys. Oceanogr.*, *23*, 2493–2497, 1993.

Watts, D. R., C. Sun, and S. Rintoul, A two-dimensional gravest empirical modes determined from hydrographic observations in the Subantarctic Front, *J. Phys. Oceanogr.*, *31*, 2186–2209, 2001.

C. Sun, Geophysical Fluid Dynamic Laboratory/National Oceanic and Atmospheric Administration, P. O. Box 308, Princeton, NJ 08542, USA. (cns@gfdl.noaa.gov)

D. R. Watts, Graduate School of Oceanography, University of Rhode Island, Narragansett, RI 02882, USA. (rwatts@gso.uri.edu)